HHS Public Access

Author manuscript

J Magn Reson Imaging. Author manuscript; available in PMC 2018 April 01.

Published in final edited form as:

J Magn Reson Imaging. 2018 April ; 47(4): 995–1002. doi:10.1002/jmri.25845.

MRI Proton Density Fat Fraction Is Robust Across the Biologically Plausible Range of Triglyceride Spectra in Adults With Nonalcoholic Steatohepatitis

Cheng William Hong, MD, MS[1], **Adrija Mamidipalli, MBBS**[1], **Jonathan C. Hooker, BS**[1], **Gavin Hamilton, PhD**[1], **Tanya Wolfson, MA**[2], **Dennis H. Chen, BSE**[1], **Soudabeh Fazeli Dehkordy, MD, MPH**[1], **Michael S. Middleton, MD, PhD**[1], **Scott B. Reeder, MD, PhD**[3], **Rohit Loomba, MD, MHSc**[4], and **Claude B. Sirlin, MD**[1,*]

[1]Liver Imaging Group, Department of Radiology, University of California San Diego, San Diego, California, USA

[2]Computational and Applied Statistics Laboratory, University of California San Diego, San Diego, California, USA

[3]Departments of Radiology, Medical Physics, Biomedical Engineering, Medicine, and Emergency Medicine, University of Wisconsin Madison, Madison, Wisconsin

[4]NAFLD Research Center, Division of Gastroenterology, Department of Medicine, University of California San Diego, San Diego, California, USA

Abstract

Background—Proton density fat fraction (PDFF) estimation requires spectral modeling of the hepatic triglyceride (TG) signal. Deviations in the TG spectrum may occur, leading to bias in PDFF quantification.

Purpose—To investigate the effects of varying six-peak TG spectral models on PDFF estimation bias.

Study Type—Retrospective secondary analysis of prospectively acquired clinical research data.

Population—Forty-four adults with biopsy-confirmed nonalcoholic steatohepatitis.

Field Strength/Sequence—Confounder-corrected chemical-shift-encoded 3T MRI (using a 2D multiecho gradient-recalled echo technique with magnitude reconstruction) and MR spectroscopy.

Assessment—In each patient, 61 pairs of colocalized MRI-PDFF and MRS-PDFF values were estimated: one pair used the standard six-peak spectral model, the other 60 were six-peak variants calculated by adjusting spectral model parameters over their biologically plausible ranges. MRI-PDFF values calculated using each variant model and the standard model were compared, and the agreement between MRI-PDFF and MRS-PDFF was assessed.

*Address reprint requests to: C.B.S., Department of Radiology, University of California, San Diego, Altman Clinical and Translational Research Institute, 9452 Medical Center Dr., La Jolla, CA 92037. csirlin@ucsd.edu.

Statistical Tests—MRS-PDFF and MRI-PDFF were summarized descriptively. Bland–Altman (BA) analyses were performed between PDFF values calculated using each variant model and the standard model. Linear regressions were performed between BA biases and mean PDFF values for each variant model, and between MRI-PDFF and MRS-PDFF.

Results—Using the standard model, mean MRS-PDFF of the study population was 17.9±8.0% (range: 4.1–34.3%). The difference between the highest and lowest mean variant MRI-PDFF values was 1.5%. Relative to the standard model, the model with the greatest absolute BA bias overestimated PDFF by 1.2%. Bias increased with increasing PDFF ($P < 0.0001$ for 59 of the 60 variant models). MRI-PDFF and MRS-PDFF agreed closely for all variant models (R^2=0.980, $P < 0.0001$).

Data Conclusion—Over a wide range of hepatic fat content, PDFF estimation is robust across the biologically plausible range of TG spectra. Although absolute estimation bias increased with higher PDFF, its magnitude was small and unlikely to be clinically meaningful.

Level of Evidence—3

Technical Efficacy—Stage 2

MRI-based proton density fat fraction (PDFF), the leading imaging biomarker to noninvasively quantify hepatic steatosis,[1–7] correlates strongly with histologic grade of hepatic steatosis[8–10] and with PDFF measured by single-voxel MR spectroscopy (MRS).[11–17] To quantify MRI-PDFF, confounder-corrected chemical-shift-encoded MRI (CSE-MRI) methods are utilized. These are typically acquired using a low flip angle to minimize T_1 bias and multiple echo times to encode fat-water signal oscillation and correct for $R2^* (1/T_2^*)$ signal decay, providing simultaneous estimates of PDFF and R2*. It is well established that estimating PDFF from echoes acquired at multiple echo times requires a multipeak spectral fat model to accurately characterize the signal from triglycerides (TG).[12,18–21] Similarly, multipeak spectral modeling is also required to accurately estimate R2*.[22] The raw data for each voxel can then be used to calculate PDFF maps using either magnitude or complex data-based techniques.[23,24]

Since MRI-PDFF estimation does not directly measure the fat spectrum, it requires a priori knowledge of this spectrum. Although there are nine distinct proton moieties in the TG molecule, several resonances (5.29 and 5.19 ppm, 2.20 and 2.02 ppm, 1.6 and 1.3 ppm) are not resolvable in vivo at clinical field strengths, and the observable fat spectrum has six distinct peaks.[25] The most commonly used sixpeak fat spectral model was derived by Hamilton et al[25] from in vivo spectroscopy and knowledge of the TG molecular structure, which is determined by three parameters: the chain length (CL), number of double bonds (NDB) per molecule, and number of methylene-interrupted double bonds (NMIDB).

While this model has been applied in various research studies[12,13,25,26] and is used in some commercial MRI-based techniques for fat quantification, other spectral models have been proposed. These include a three-peak model described by Yu et al,[21] four- and five-peak models described by Wokke et al,[27] a seven-peak model described by Ren et al,[28] and a nine-peak model described by Hamilton et al.[25] Thus, there is uncertainty regarding the optimal spectral model to use. In addition, due to variation in TG composition in fat depots

in the body and across individuals,[29] a single spectral model may not apply in all situations. Deviations of the true fat spectrum from the assumed fat spectrum may result in quantification bias using MRI-based techniques.

The purpose of this study was to assess the effect of varying six-peak spectral models on MRI-PDFF estimation bias and on agreement with MRS-PDFF. A secondary aim of this study was to assess the effect of varying spectral models on R2* estimation.

Materials and Methods

Study Design

This was a secondary analysis of a prospective clinical trial studying the effect of ezetimibe on hepatic PDFF in adults with biopsyconfirmed nonalcoholic steatohepatitis (NASH).[3] The study was approved by an Institutional Review Board and was compliant with the Health Insurance Portability and Accountability Act. Informed consent was obtained from all patients. Detailed inclusion and exclusion criteria for this clinical study has been previously published.[3] The parent study enrolled 50 patients, but five were excluded from the present analysis because MRS was not performed, and one was excluded due to a severe parallel imaging artifact degrading the images at the exact location of the MRS voxel. As such, 44 patients were included in this analysis (27 female, 17 male), with a mean age of 49±15 years (range: 19–75 years). Patients underwent confounder-corrected CSE-MRI and multiecho MRS examinations at 3T. CSE-MRI was used to estimate MRI-PDFF and R2*, and MRS was used to estimate MRS-PDFF. Demographical and anthropometric information was collected for all patients. For this analysis, only the baseline examinations were used.

MRI Acquisition

Patients were scanned supine using a 3T MRI system (Signa EXCITE HDxt scanner, GE Healthcare, Waukesha, WI) with an eight-channel torso phased-array coil centered over the liver. A dielectric pad was placed between the coil and the abdomen.

A 2D multiecho spoiled gradient-recalled echo (SPGR) sequence was acquired with full liver coverage in one or two 18–30-second breath-holds. A low flip angle (10°) with ≥150 msec repetition time (TR) was used to minimize T_1 bias.[11,14,16,20] Six echoes were obtained per TR at nominally out-of-phase and in-phase echo times (based on a methylene resonance of 434 Hz relative to the water peak) of 1.15, 2.3, 3.45, 4.6, 5.75, and 6.9 msec to permit estimation of R2*-corrected PDFF and fat-corrected R2*, assuming exponential decay. A previously described fitting algorithm was applied to the source images pixel-by-pixel to create parametric PDFF maps.[20] The rectangular field of view was adjusted depending on the patient's body habitus and breath-hold capacity. Due to the fat-water ambiguity intrinsic to magnitude fitting, water was assumed to be the dominant signal and the PDFF dynamic range was limited to 0–50%. No corrections were necessary for phase errors.[26,30] as reconstruction of PDFF maps was performed with magnitude fitting. Externally calibrated (ASSET) parallel imaging was applied in the phase-encoding direction with a net acceleration factor of 1.25. MRI parameters are summarized in Table 1.

MRI and Spectral Model Analysis

MRI-PDFF was estimated by placing regions-of-interest (ROIs) of 1-cm radius on three consecutive axial slices colocalized to the MRS voxel location. Three slices were used since the MRS voxel is thicker than the individual slices. As described in previous studies, [4,13,31] placing ROIs in this way allows comparison of PDFF estimated from MRI and MRS. Mean signal intensities in those ROIs were recorded and used to estimate PDFF and R2* using the standard Hamilton model for fat spectral modeling.[25] This model assumes a CL of 17.45, NDB of 1.92, and NMIDB of 0.32, which corresponds to relative amplitudes of 4.7%, 3.9%, 0.6%, 12.0%, 70.0%, and 8.8% at the fat peaks corresponding to 5.3, 4.2, 2.75, 2.1, 1.3, and 0.9 ppm, respectively.

In addition, 60 variant six-peak spectral models were generated by varying CL, NDB, and NMIDB between 17.35–17.55 (increments of 0.1), 1.9–2.7 (increments of 0.2), and 0.3–0.9 (increments of 0.2) and recomputing the corresponding relative amplitudes of the fat spectral model.[29] We determined the biologically plausible ranges for those three parameters by selecting ranges that would include all previously described spectral models [21,25,27,28] and also correspond to physically possible molecular structures (eg, NMIDB must be less than or equal to NDB −1). PDFF and R2* values in each ROI then were computed for each variant model by entering the recomputed relative amplitudes into the fitting algorithm. Goodness-of-fit, assessed with R^2 values, were also computed for each of the spectral models for each fitting performed. For each patient, MRI-PDFF and R2* values in the three ROIs were averaged for the standard model and separately for each of the 60 variant models.

For illustrative purposes, MRI-PDFF maps were generated with a single peak model of fat, with the standard six-peak spectral model, and with variant spectral models causing the greatest over-estimation and greatest underestimation relative to the standard model.

MRS Acquisition and Analysis

MRS-PDFF was measured as internal validation for the accuracy of MRI-PDFF measurements.[7] MRS was performed using a stimulated echo acquisition mode (STEAM) sequence, as described by Hamilton et al.[25] In brief, for each patient, a $2 \times 2 \times 2$ cm^3 MRS voxel was placed in the right hepatic lobe, with a localizing axial image stored showing the MRS voxel position. The voxel was shimmed during free breathing before single breath-hold acquisition of long-TR (3500 msec), multi-TE STEAM MRS. No frequency or spatial saturation was applied. Five spectra were acquired consecutively at progressively longer TEs of 10, 15, 20, 25, and 30 msec to permit T_2 correction. Spectra collected from each of the eight surface coil elements were combined using singular value decomposition.[32] Spectral analysis was performed using the AMARES algorithm included in the MRUI software packages, [33,34] and the fat peaks were modeled with multiple Gaussian resonances.[25] When fitting spectra, the frequency of fat peaks was fixed relative to each other, but not to water, and the linewidth and peak area of all peaks was unconstrained, with no spectral model assumed. Both the standard and 60 variant MRS-PDFF values were estimated by using the same spectral models as used with MRI. This was done by adjusting the relative amplitudes of the fat peaks at 5.3 ppm and 4.2 ppm (the two fat peaks hidden by the water peak at 3T) as appropriate for the changes in assumed CL and NDB; no adjustment was needed for

changes in assumed NMIDB, which has no effect on the 5.3 and 4.2 ppm fat peaks.[25] MRS-PDFF was estimated as the ratio of fat signal to the sum of fat and water signals.

Statistical Analysis

Statistical analysis was performed using R v. 3.3.3 statistical software (2016; R Foundation for Statistical Computing, Vienna, Austria). A significance level of 0.05 was used for all statistical testing. Demographical information was summarized descriptively.

The effect of modifying CL, NDB, and NMIDB on variant PDFF values was examined by computing the mean MRI-PDFF values for each variant spectral model over all patients. The R^2 values of the fits were summarized descriptively. Bland–Altman analysis was performed between the variant PDFF and standard PDFF values. Linear regression was then performed with the bias (difference between the variant PDFF and standard PDFF) as the outcome variable, and the baseline PDFF (average of variant PDFF and standard PDFF) for each variant spectral model. The agreement between corrected MRS-PDFF and colocalized variant MRI-PDFF was assessed using simple linear regression on data acquired from all spectral models.

R2* values were also computed for each spectral model for each patient. The agreement between standard R2* values and variant R2* values were assessed using linear regression over all spectral models.

Results

Study Population

In the study population, using the standard spectral model, the mean MRS-PDFF (reference standard) was 18.1±8.1% (range: 4.1–34.3%), and the mean colocalized MRI-PDFF was 17.6±8.4% (range: 4.6–34.3%).

Effect of Each Parameter

Estimated MRI-PDFF increased with increasing NDB, but decreased with increasing CL and NMIDB (Table 2). Changes in the assumed NDB had a greater impact on PDFF estimation than changes in the assumed CL or NMIDB. For example, changing the NDB across its biologically plausible range caused the mean PDFF to change by 1.15–1.18%, depending on the assumed CL and NMIDB; by comparison, changing the NMIDB across its biologically plausible range caused the mean PDFF to change by 0.29–0.31%, depending on the assumed CL and NDB (Fig. 1). For any given pair of assumed NDB and NMIDB, changing the CL across its biologically plausible range caused the mean PDFF to change by 0.06–0.09%, depending on the assumed NDB and NMIDB. The highest and lowest variant PDFF values averaged over all patients across the range of spectral models differed by 1.5% (18.8% and 17.3%, respectively). The model with the highest bias relative to the standard model assumed a CL of 17.35, NDB of 2.7, and NMIDB of 0.3; this model had a bias of +1.2% (limits of agreement [LOA]: –0.5% to+1.9%). All spectral models fit the signal data well, with mean R^2 values ranging from 0.992–0.996. Qualitatively, reconstructed PDFF maps

had similar appearance across the full range of biologically plausible spectral models (Fig. 2).

Bland–Altman Analyses

Bias in PDFF estimation increased with increasing baseline PDFF (Fig. 3). Mean bias of all variant spectral models was +0.4% (LOA: –0.5% to+1.4%). Linear regressions for all variant spectral models demonstrated bias increased with increasing baseline PDFF ($P < 0.0001$ for 59 of 60 variant models, $R^2 > 0.90$ for 56 of 60 variant models). The mean slope for these 60 regressions was 0.0174 ± 0.0165 (range: –0.0113 to 0.0461).

Correlation With MRS

As with MRI, MRS-PDFF increased with increasing NDB, but decreased with increasing CL (Table 3). The variant MRS-PDFF values were independent of NMIDB, as NMIDB does not affect the amplitudes of the 5.3 ppm and 4.2 ppm peaks. Mean MRS-PDFF values obtained from each of the models ranged from 18.0–18.4%. For each spectral model, the mean difference between colocalized MRI-PDFF and MRS-PDFF was computed, and the range of mean differences was –0.76% to 0.40%. Linear regression between the variant MRS-PDFF values and the colocalized variant MRI-PDFF values demonstrated high agreement over all models (Fig. 4, R^2=0.980, $P < 0.0001$).

Estimation of R2* With Varying Spectral Model of Fat

MRI-R2* estimated using variant spectral models agreed closely with MRI-R2* estimated using the standard model (Fig. 5, R^2=0.997, $P < 0.0001$).

Discussion

This study demonstrates that although the estimation of PDFF and R2* using CSE-MRI requires the use of a multi-peak spectral model of fat, all biologically plausible models that were tested had only a small effect on estimated PDFF and R2*. Over the biologically plausible ranges of TG spectral models, the difference between the highest and lowest mean PDFF estimated by variant models was 1.5%, and the model with the largest bias compared to the standard model had an average bias of +1.2%. This bias is probably not clinically meaningful in most instances, although it may be relevant if reliable detection of slight differences is desired, such as subtle spatial distribution heterogeneity at a cross-sectional timepoint or small but real longitudinal changes, where the TG chemical structure may change over time. In those situations, one potential solution to uncertainty in the TG spectral model is to simultaneously estimate PDFF and the fat composition parameters (NDB, NMIDB, and CL), although this is currently not commonly done in clinical practice.[35,36] The finding that the bias associated with varying spectral models is small also suggests that PDFF estimated using different spectral models may be pooled in meta-analyses, provided that the PDFF estimations were done in a similar manner as in our study. Similarly, we found only minor bias in R2* estimation over the biologically plausible range of six-peak spectral models.

Based on knowledge of the triglyceride molecular structure, the relative amplitudes of the six peaks visible at in vivo field strengths can be specified by three parameters: the CL, NDB, and NMIDB. Thus, by varying CL, NDB, and NMIDB across the biologically plausible range, all biologically plausible six-peak spectral models are encompassed.

The subsequent linear regressions over this range of spectral models found that baseline PDFF was highly associated with Bland–Altman bias, except for a few models that were similar to the standard six-peak spectral model and had almost no bias. Because the effect of varying fat spectral models depends on the baseline PDFF, the choice of specific spectral model has a larger absolute impact at higher fat fractions. Even then, the bias remains relatively low. Of the three parameters that specify the spectral model, NDB, which reflects the degree of saturation of the fatty acid chains in TG, had the greatest effect on PDFF estimation. Based on Hamilton et al, this is to be expected: NDB affects the modeled amplitude of widely spaced peaks (ranging from 5.29 to 1.30 ppm), and therefore has a larger effect on fat-water signal interference, while NMIDB affects the modeled amplitude of only closed spaced peaks (ranging from 2.75 to 1.30 ppm), and therefore has a smaller effect on modeled fat-water signal interference.[25] Contributing to the modeled amplitude of only one peak (1.30 ppm) and with a narrow biologically plausible range, CL has the smallest effect on PDFF estimation. Because variations in the spectral model have small effects on PDFF estimation, characterization of adipose tissue composition using CSE-MRI methods may be challenging, especially in the determination of NMIDB and CL, which have even smaller effects on modeled fat-water signal interference than NDB.

MRS has been used as a reference standard for MRI in various previous studies. This is corroborated in our analysis, as the association between MRS and colocalized MRI is high regardless of the selected spectral model. Wang et al previously demonstrated that PDFF estimation using seven different published multipeak fat spectral models had comparable accuracy.[37] The results here support their finding in an independent cohort, and add to it by demonstrating that any six-peak fat spectral model within the biologically plausible range provides excellent agreement between MRI and MRS. In order for MRS to be an appropriate reference standard for MRI, the same spectral model should be applied. However, Fig. 3 demonstrates that even in a worst-case scenario in which points in each ellipse containing the distribution of possible PDFF estimates are intentionally chosen to maximize MRI-MRS disagreement, agreement would still remain high because the sizes of the ellipses are very small.

We also found that MRS was more robust than MRI to changes in the spectral model. This is also an expected finding, since the spectral model plays a smaller role in MRS compared to MRI. MRS only applies the spectral model to determine the relative amplitudes of the 5.3 and 4.2 ppm peaks that cannot be measured directly because they coincide with that of water, but can directly observe the other fat peaks. In comparison, the relative amplitudes of the fat peaks between 0–3 ppm have to be specified a priori by the spectral model when using MRI.

One limitation of this study was its small sample size. Another was that our emphasis on magnitude-based PDFF limits generalizability to complex-based[24,38–41] methods. This also

limits the applicability of our findings to other tissues such as bone marrow or adipose tissue, where the full PDFF dynamic range of 0–100% provided by complex-based methods is needed. We only studied one framework of PDFF estimation using six echoes, six-peak spectral models, and an echo time spacing of 1.15 msec at 3T, and our results may not generalize to PDFF estimated using different acquisition parameters or reconstruction methods. As this was a secondary analysis of adults with biopsy-proven NASH recruited at a single tertiary academic center for a prospective clinical trial, further work is needed to affirm the generalizability of our results to children, populations in other geographic regions, and adults without NASH. Lastly, because the true TG spectral model at the MRS location was not known, we were not able to quantify the absolute error attributable to changes in the spectral model, and could only determine the variation in PDFF estimation.

In conclusion, the effect of varying the TG spectral model on PDFF estimation using both MRI and MRS is minimal. Greater bias is seen at higher fat fractions, but remains low. MRI and MRS demonstrate excellent agreement across the range of biologically plausible multipeak fat spectral models. As such, within the range of fat content observed in the liver, PDFF estimation is robust to biologically plausible TG compositions, further supporting its use as an imaging biomarker of liver fat content. Even if PDFF is estimated in different anatomic locations or across individuals where variations in TG spectrum from the assumed spectrum may be present, the effect on PDFF estimation is likely to be minimal. Finally, the robustness of PDFF estimation across TG spectral models helps justify direct comparison of and aggregation for meta-analyses of published results obtained with different models.

Acknowledgments

Contract grant sponsor: National Institutes of Health; contract grant numbers: T32 EB005970-09, R01 DK106419-02, R01 DK083380, K24 DK102595, R01 DK088925, and R01 DK100651-03

We thank GE Healthcare, who provides research support to UCSD and UW-Madison.

References

1. Noureddin M, Lam J, Peterson MR, et al. Utility of magnetic resonance imaging versus histology for quantifying changes in liver fat in nonalcoholic fatty liver disease trials. Hepatology. 2013; 58:1930–1940. [PubMed: 23696515]
2. Bacchi E, Negri C, Targher G, et al. Both resistance training and aerobic training reduce hepatic fat content in type 2 diabetic subjects with nonalcoholic fatty liver disease (the RAED2 Randomized Trial). Hepatology. 2013; 58:1287–1295. [PubMed: 23504926]
3. Loomba R, Sirlin CB, Ang B, et al. Ezetimibe for the treatment of non-alcoholic steatohepatitis: Assessment by novel magnetic resonance imaging and magnetic resonance elastography in a randomized trial (MOZART trial). Hepatology. 2015; 61:1239–1250. [PubMed: 25482832]
4. Le T-A, Chen J, Changchien C, et al. Effect of colesevelam on liver fat quantified by magnetic resonance in nonalcoholic steatohepatitis: A randomized controlled trial. Hepatology. 2012; 56:922–932. [PubMed: 22431131]
5. Tang A, Rabasa-Lhoret R, Castel H, et al. Effects of insulin glargine and liraglutide therapy on liver fat as measured by magnetic resonance in patients with type 2 diabetes: A randomized trial. Diabetes Care. 2015; 38:1339–1346. [PubMed: 25813773]
6. Reeder SB, Hu HH, Sirlin CB. Proton density fat-fraction: A standardized MR-based biomarker of tissue fat concentration. J Magn Reson Imaging. 2012; 36:1011–1014. [PubMed: 22777847]

7. Reeder SB, Cruite I, Hamilton G, Sirlin CB. Quantitative assessment of liver fat with magnetic resonance imaging and spectroscopy. J Magn Reson Imaging. 2011; 34:729–749. [PubMed: 21928307]
8. Idilman IS, Aniktar H, Idilman R, et al. Hepatic steatosis: Quantification by proton density fat fraction with MR imaging versus liver biopsy. Radiology. 2013; 267:767–775. [PubMed: 23382293]
9. Permutt Z, Le TA, Peterson MR, et al. Correlation between liver histology and novel magnetic resonance imaging in adult patients with non-alcoholic fatty liver disease — MRI accurately quantifies hepatic steatosis in NAFLD. Aliment Pharmacol Ther. 2012; 36:22–29. [PubMed: 22554256]
10. Tang A, Tan J, Sun M, et al. Nonalcoholic fatty liver disease: MR imaging of liver proton density fat fraction to assess hepatic steatosis. Radiology. 2013; 267:422–431. [PubMed: 23382291]
11. Yokoo T, Bydder M, Hamilton G, et al. Nonalcoholic fatty liver disease: Diagnostic and fat-grading accuracy of low-flip-angle multiecho gradient-recalled-echo MR imaging at 1. 5 T. Radiology. 2009; 251:67–76. [PubMed: 19221054]
12. Meisamy S, Hines CDG, Hamilton G, et al. Quantification of hepatic steatosis with T1-independent, T2-corrected MR imaging with spectral modeling of fat: Blinded comparison with MR spectroscopy. Radiology. 2011; 258:767–775. [PubMed: 21248233]
13. Hines CDG, Frydrychowicz A, Hamilton G, et al. T(1) independent, T(2) (*) corrected chemical shift based fat-water separation with multipeak fat spectral modeling is an accurate and precise measure of hepatic steatosis. J Magn Reson Imaging. 2011; 33:873–881. [PubMed: 21448952]
14. Yokoo T, Shiehmorteza M, Hamilton G, et al. Estimation of hepatic proton-density fat fraction by using MR imaging at 3. 0 T. Radiology. 2011; 258:749–759. [PubMed: 21212366]
15. Zhong X, Nickel MD, Kannengiesser SAR, Dale BM, Kiefer B, Bashir MR. Liver fat quantification using a multi-step adaptive fitting approach with multi-echo GRE imaging. Magn Reson Med. 2014; 72:1353–1365. [PubMed: 24323332]
16. Kühn J-P, Hernando D, Mensel B, et al. Quantitative chemical shiftencoded MRI is an accurate method to quantify hepatic steatosis. J Magn Reson Imaging. 2014; 39:1494–1501. [PubMed: 24123655]
17. Pirasteh, A., Bashir, MR., Reeder, SB., et al. Linearity, bias, and precision of proton-density fat fraction for liver fat quantification: A meta-analysis. Proc 25th Annual Meeting ISMRM; Honolulu. 2017.
18. Reeder SB, Brittain JH, Grist TM, Yen Y-F. Least-squares chemical shift separation for13C metabolic imaging. J Magn Reson Imaging. 2007; 26:1145–1152. [PubMed: 17896366]
19. Reeder SB, Robson PM, Yu H, et al. Quantification of hepatic steatosis with MRI: The effects of accurate fat spectral modeling. J Magn Reson Imaging. 2009; 29:1332–1339. [PubMed: 19472390]
20. Bydder M, Yokoo T, Hamilton G, et al. Relaxation effects in the quantification of fat using gradient echo imaging. Magn Reson Imaging. 2008; 26:347–359. [PubMed: 18093781]
21. Yu H, Shimakawa A, McKenzie CA, Brodsky E, Brittain JH, Reeder SB. Multiecho water-fat separation and simultaneous R2* estimation with multifrequency fat spectrum modeling. Magn Reson Med. 2008; 60:1122–1134. [PubMed: 18956464]
22. Kühn J-P, Hernando D, Muñoz del Rio A, et al. Effect of multipeak spectral modeling of fat for liver iron and fat quantification: Correlation of biopsy with MR imaging results. Radiology. 2012; 265:133–142. [PubMed: 22923718]
23. Reeder SB, Sirlin CB. Quantification of liver fat with magnetic resonance imaging. Magn Reson Imaging Clin N Am. 2010; 18:337–357. ix. [PubMed: 21094444]
24. Reeder SB, Pineda AR, Wen Z, et al. Iterative decomposition of water and fat with echo asymmetry and least-squares estimation (IDEAL): Application with fast spin-echo imaging. Magn Reson Med. 2005; 54:636–644. [PubMed: 16092103]
25. Hamilton G, Yokoo T, Bydder M, et al. In vivo characterization of the liver fat ^{1}H MR spectrum. NMR Biomed. 2011; 24:784–790. [PubMed: 21834002]
26. Hernando D, Hines CDG, Yu H, Reeder SB. Addressing phase errors in fat-water imaging using a mixed magnitude/complex fitting method. Magn Reson Med. 2012; 67:638–644. [PubMed: 21713978]

27. Wokke BH, Bos C, Reijnierse M, et al. Comparison of dixon and T1-weighted MR methods to assess the degree of fat infiltration in Duchenne muscular dystrophy patients. J Magn Reson Imaging. 2013; 38:619–624. [PubMed: 23292884]
28. Ren J, Dimitrov I, Sherry AD, Malloy CR. Composition of adipose tissue and marrow fat in humans by 1H NMR at 7 Tesla. J Lipid Res. 2008; 49:2055–2062. [PubMed: 18509197]
29. Hamilton G, Schlein AN, Middleton MS, et al. In vivo triglyceride composition of abdominal adipose tissue measured by (1) H MRS at 3T. J Magn Reson Imaging. 2017; 45:1455–1463. [PubMed: 27571403]
30. Yu H, Shimakawa A, Hines CDG, et al. Combination of complex-based and magnitude-based multiecho water-fat separation for accurate quantification of fat-fraction. Magn Reson Med. 2011; 66:199–206. [PubMed: 21695724]
31. Tyagi A, Yeganeh O, Levin Y, et al. Intra- and inter-examination repeatability of magnetic resonance spectroscopy, magnitude-based MRI, and complex-based MRI for estimation of hepatic proton density fat fraction in overweight and obese children and adults. Abdom Imaging. 2015; 40:3070–3077. [PubMed: 26350282]
32. Bydder M, Hamilton G, Yokoo T, Sirlin CB. Optimal phased-array combination for spectroscopy. Magn Reson Imaging. 2008; 26:847–850. [PubMed: 18486392]
33. Vanhamme, van den Boogaart A, Van Huffel S. Improved method for accurate and efficient quantification of MRS data with use of prior knowledge. J Magn Reson. 1997; 129:35–43. [PubMed: 9405214]
34. Naressi A, Couturier C, Devos JM, et al. Java-based graphical user interface for the MRUI quantitation package. MAGMA. 2001; 12:141–152. [PubMed: 11390270]
35. Peterson P, Ma°nsson S. Simultaneous quantification of fat content and fatty acid composition using MR imaging. Magn Reson Med. 2013; 69:688–697. [PubMed: 22532403]
36. Leporq B, Lambert SA, Ronot M, Vilgrain V, Van Beers BE. Quantification of the triglyceride fatty acid composition with 3. 0?T. MRI NMR Biomed. 2014; 27:1211–1221. [PubMed: 25125224]
37. Wang X, Hernando D, Reeder SB. Sensitivity of chemical shiftencoded fat quantification to calibration of fat MR spectrum. Magn Reson Med. 2016; 75:845–851. [PubMed: 25845713]
38. Reeder SB, Wen Z, Yu H, et al. Multicoil Dixon chemical species separation with an iterative least-squares estimation method. Magn Reson Med. 2004; 51:35–45. [PubMed: 14705043]
39. Reeder SB, McKenzie CA, Pineda AR, et al. Water-fat separation with IDEAL gradient-echo imaging. J Magn Reson Imaging. 2007; 25:644–652. [PubMed: 17326087]
40. Hernando D, Haldar JP, Sutton BP, Ma J, Kellman P, Liang Z-P. Joint estimation of water/fat images and field inhomogeneity map. Magn Reson Med. 2008; 59:571–580. [PubMed: 18306409]
41. Bashir MR, Zhong X, Nickel MD, et al. Quantification of hepatic steatosis with a multistep adaptive fitting MRI approach: Prospective validation against MR spectroscopy. Am J Roentgenol. 2015; 204:297–306. [PubMed: 25615751]

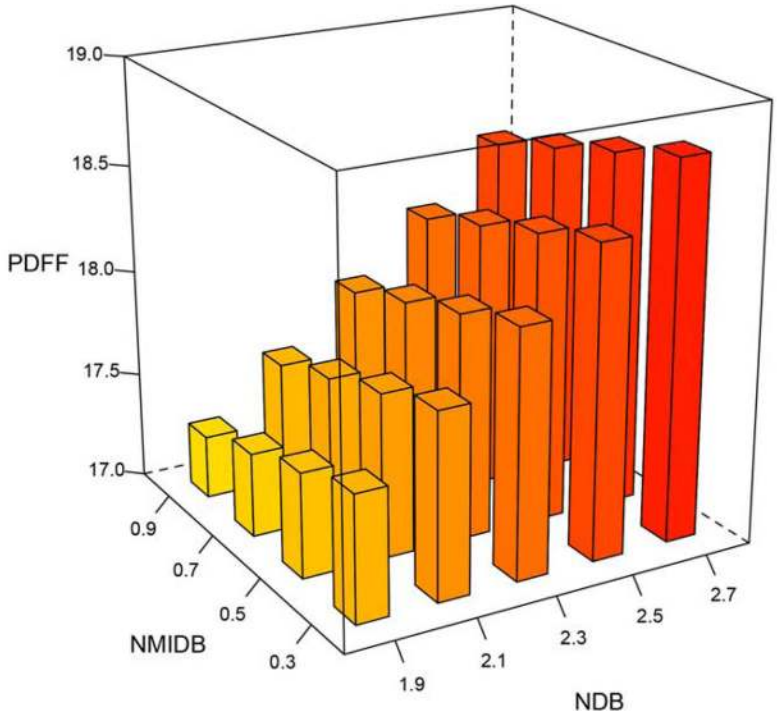

FIGURE 1.

3D bar plot demonstrating mean PDFF vs. NDB and NMIDB, averaged over the range of CL between 17.35 and 17.55. These values depict the mean PDFF across the study cohort. Each bar is colored based on its height (lower to higher PDFF values depicted using yellow to red). Changes in the assumed NDB had a greater impact on PDFF estimation than changes in the assumed NMIDB.

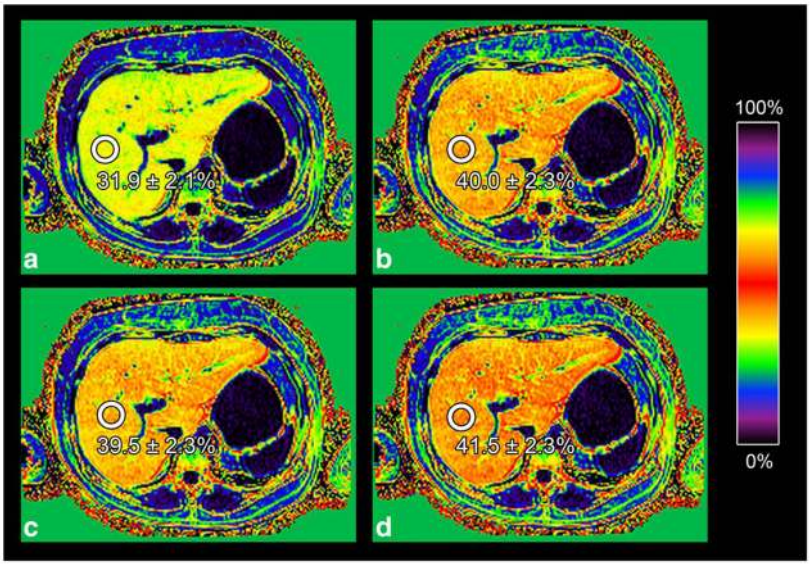

FIGURE 2.

Four PDFF maps reconstructed (a) using a single peak model, (b) using the standard six-peak spectral model, (c) using the sixpeak spectral model which computed the lowest PDFF values, and (d) using the six-peak spectral model which computed the highest PDFF values. The PDFF map reconstructed using a single peak model appears noticeably darker and corresponds to a substantial under-estimation of the true fat fraction, but the maps reconstructed with six-peak spectral models appear visually similar over the range of biologically plausible spectral models. ROIs (white circles), PDFF values, and standard deviations are also shown. Notice that because we used a magnitude-based reconstruction technique, there is signal dominance ambiguity as illustrated in the color lookup table.

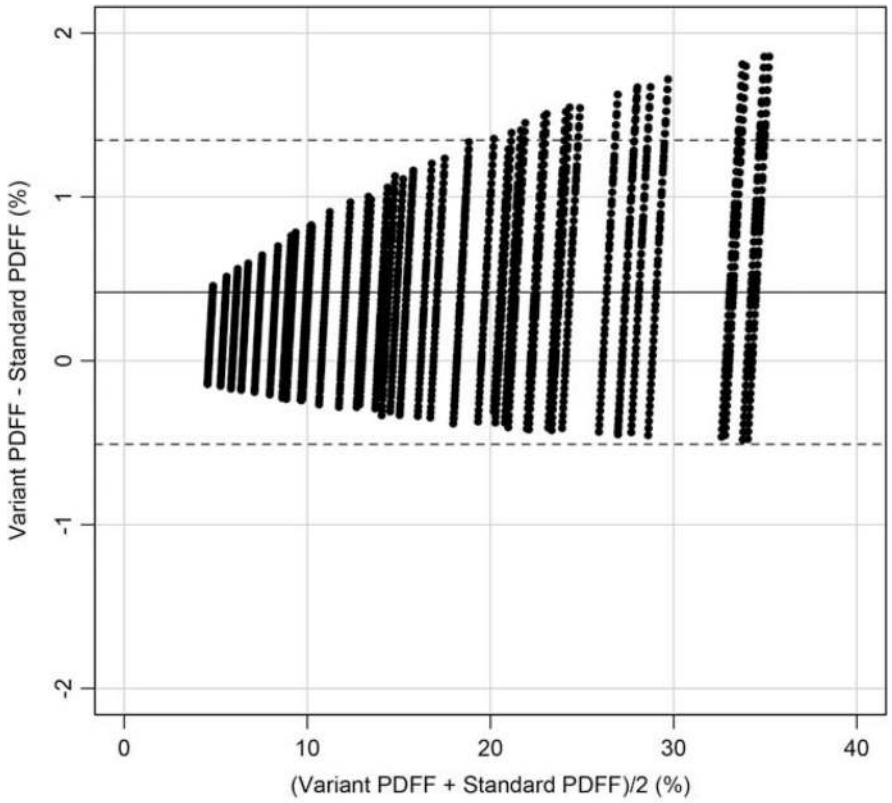

FIGURE 3.

Bland–Altman bias between variant and standard PDFF vs. the mean of variant and standard PDFF, over all spectral models. Mean bias (solid line) and limits of agreement (dashed lines) are shown. Bias increased as PDFF increased, demonstrating that varying spectral models resulted in variation proportional to the baseline PDFF.

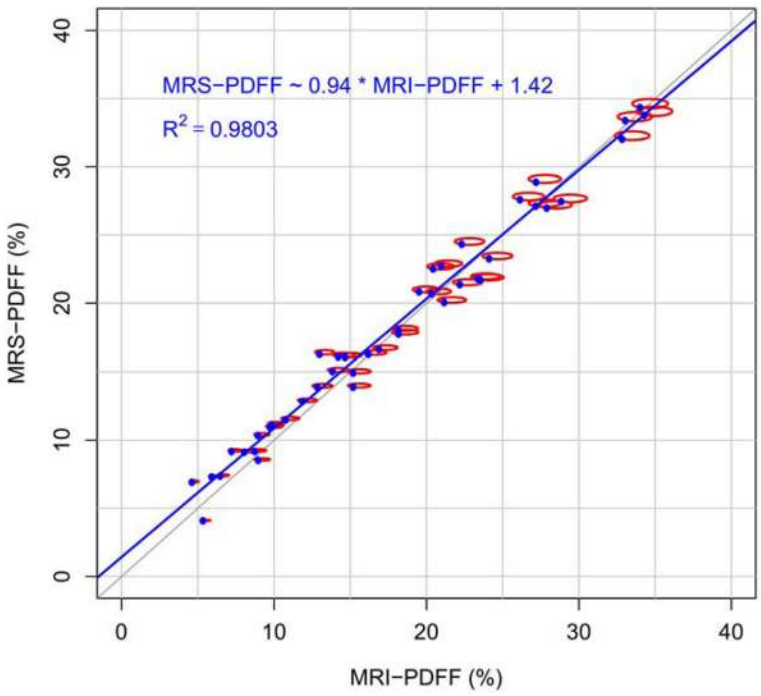

FIGURE 4.

Corrected MRS-PDFF vs. variant MRI-PDFF. Each ellipse (red) represents a patient, and the size of the ellipse represents the range of MRS-PDFF and MRI-PDFF values obtained from the full range of spectral models. The light gray line is the identity line of y=x, and the solid blue line is the least squares linear regression line between the MRS-PDFF and MRI-PDFF values derived from the standard Hamilton model (blue dots). All spectral models analyzed in this study provided excellent agreement between PDFF measurements from MRI and MRS.

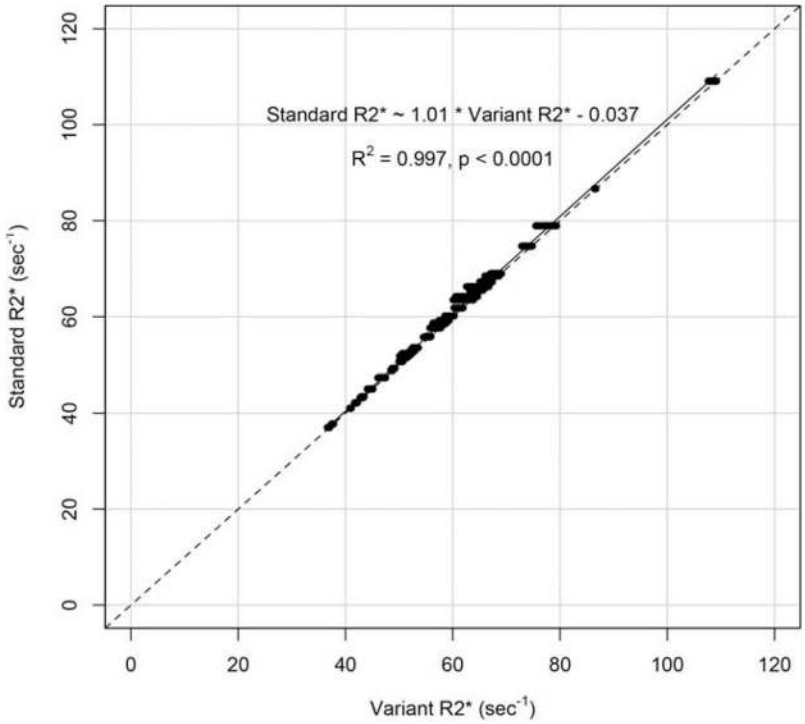

FIGURE 5.

Standard R2* vs. variant R2*. For each patient and each variant spectral model obtained by varying NDB, NMIDB, and CL, the R2* estimated from that variant spectral model is plotted against the R2* estimated by the standard spectral model for that patient. The dashed line is the identity line of y=x, and the solid black line is the least squares linear regression line. There is close agreement between R2* values estimated from the standard and variant spectral models.

TABLE 1

MRI Parameters for Confounder-Corrected Chemical-Shift-Encoded Magnitude-Based Proton Density Fat Fraction Multiecho GRE Sequence

Parameter	Range of values
Pulse sequence	2D Spoiled GRE
TR (msec)	225–275
Number of echoes per TR	6
TE (msec)	1.15, 2.3, 3.45, 4.6, 5.75, 6.9
Matrix size	224 × 128
Flip angle (°)	10
Percent phase field of view (%)	75–90
Reconstruction diameter (mm)	400–480
Slice thickness (mm)	8
Number of averages	1
Parallel imaging	Externally calibrated, R=1.25 in phase direction
Gap between slices (mm)	0

GRE=gradient recalled echo; TR=repetition time; TE=echo time.

TABLE 2

Mean MRI-PDFF Values Across the Study Cohort

	NDB				
NMIDB	**1.9**	**2.1**	**2.3**	**2.5**	**2.7**
CL=17.35					
0.3	17.62%	17.90%	18.19%	18.49%	**18.80%**
0.5	17.52%	17.80%	18.09%	18.39%	18.70%
0.7	17.42%	17.70%	17.99%	18.29%	18.59%
0.9	17.32%	17.60%	17.89%	18.18%	18.49%
CL=17.45					
0.3	17.59%	17.86%	18.15%	18.45%	18.75%
0.5	17.49%	17.77%	18.05%	18.35%	18.65%
0.7	17.39%	17.67%	17.95%	18.25%	18.55%
0.9	17.29%	17.57%	17.85%	18.14%	18.45%
CL=17.55					
0.3	17.55%	17.83%	18.11%	18.41%	18.71%
0.5	17.46%	17.73%	18.02%	18.31%	18.61%
0.7	17.36%	17.63%	17.92%	18.21%	18.51%
0.9	**17.26%**	17.54%	17.82%	18.11%	18.41%

Calculated by varying chain length (CL), number of double bonds (NDB), and number of methylene-interrupted double bonds (NMIDB) across their respective biologically plausible ranges. Highest and lowest mean MRI-PDFF values are depicted in bold.

TABLE 3

Mean MRS-PDFF Values Across the Study Cohort

	NDB				
CL	**1.9**	**2.1**	**2.3**	**2.5**	**2.7**
17.35	18.05%	18.13%	18.22%	18.31%	**18.39%**
17.45	18.04%	18.12%	18.21%	18.29%	18.38%
17.55	**18.03%**	18.11%	18.20%	18.28%	18.37%

Calculated by varying chain length (CL) and number of double bonds (NDB) across their respective biologically plausible ranges. Note that because MRS-PDFF is unaffected by the number of methylene-interrupted double bonds (NMIDB), it is not depicted in the table. Highest and lowest mean MRI-PDFF values are depicted in bold.